THE JOURNAL OF PHYSICAL CHEMISTRY C

Article

pubs.acs.org/JPCC

Orientation of a Series of CO_2 Reduction Catalysts on Single Crystal TiO_2 Probed by Phase-Sensitive Vibrational Sum Frequency Generation Spectroscopy (PS-VSFG)

Chantelle L. Anfuso,[†,§] Dequan Xiao,[‡,§] Allen M. Ricks,[†] Christian F. A. Negre,[‡] Victor S. Batista,*[,‡] and Tianquan Lian*[,†]

[†]Department of Chemistry, Emory University, Atlanta, Georgia 30322, United States

[‡]Department of Chemistry, Yale University, New Haven, Connecticut 06520-8107, United States

Supporting Information

ABSTRACT: We report the average molecular orientation of a series of rhenium bipyridyl CO_2 reduction catalysts adsorbed onto a rutile $TiO_2(001)$ single crystal surface. The molecular conformation of these catalysts on electrode surfaces is expected to affect their overall catalytic efficiency, since the catalytic Re center must be free to coordinate a CO_2 molecule in working systems. Phase-sensitive vibrational sum frequency generation spectroscopy (PS-VSFG) and *ab initio* SFG simulation and conformation search were used to determine the molecular tilt angles of five such complexes, $Re(L_nA)(CO)_3Cl$ [L_nA = 2,2′-bipyridine-4,4′-$(CH_2)_n$-COOH, n = 0−4] (abbreviated as ReC*n*A), as a function of the length of their anchoring groups. Results show that both the short and long axes of the catalytic bipyridine ring tilt further toward the $TiO_2(001)$ surface as the number of methylene groups in the anchoring groups increases. The increasing tilt angles are shown to correlate with an increasing conformational difference between the two anchoring groups as they lengthen, caused by the free rotation of σ-bonds between $-CH_2-$ groups. This study demonstrates an effective approach to manipulate the spatial orientation of heterogeneous electrocatalysts on TiO_2 semiconductor surfaces by varying the length of the molecular linkers.

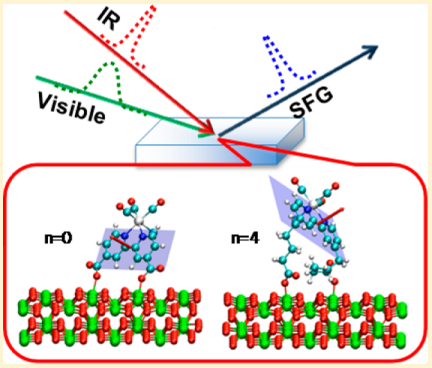

I. INTRODUCTION

Research on interfacial and surface-dependent processes has driven the development of experimental techniques capable of obtaining a detailed structural and dynamical picture of these systems. Of particular interest is the molecule−semiconductor interface, which is relevant in many types of catalytic systems, photocatalytic and photovoltaic materials, and molecular electronics.[1−5] The efficiency and specificity of many of these processes are dependent on the molecular orientation on the semiconductor surface. Determination of the molecular orientation at interfaces has proven to be experimentally challenging; however, vibrational sum frequency generation spectroscopy (VSFG) has been recognized in recent years as a useful technique for determining the average molecular conformation at interfaces.[6−9] A second-order optical technique, it is forbidden in media with inversion symmetry but allowed at interfaces where inversion symmetry is necessarily broken. This gives VSFG the distinct advantage over other optical techniques of surface specificity, and makes it an ideal tool for elucidating a molecular-level picture of molecule−semiconductor systems.

Several rhenium complexes with modified bipyridine ligands have been developed and explored in recent years for their ability to catalytically reduce CO_2 to CO.[10−18] Interestingly, a rhenium−bipyridyl complex was recently shown to have increased catalytic reductive ability when adsorbed to TiO_2 electrodes.[19] A complete understanding of the orientation and binding of these molecules to semiconductor surfaces is vital to elucidating the mechanism of electron transfer and electrocatalytic reduction.[1−3] A thorough study of the covalent attachment of these electrocatalysts on semiconductor electrodes may thus aid in the improvement and development of these catalytic materials.

Previously, our group investigated the orientation of $Re(L_0A)(CO)_3Cl$ [L_0A = 2,2′-bipyridine-4,4′-carboxylic acid] (abbreviated ReC0A) on single crystalline TiO_2 using VSFG, and found that the complex oriented roughly upright on the TiO_2 surface.[20] On the basis of these results, we wished to extend these studies on molecular orientation to include other molecules in the ReC0A family. In particular, we chose to focus on a series of five rhenium bipyridyl complexes, $Re(L_nA)(CO)_3Cl$ [L_nA = 2,2′-bipyridine-4,4′-$(CH_2)_n$-COOH, n = 0−4] (abbreviated as ReC*n*A); their structures are shown in Figure 1. These molecules are known to adsorb to semiconductor surfaces through their carboxylate anchoring groups, which are attached to the bipyridine ligands through methylene spacers of

Received: July 26, 2012
Revised: October 19, 2012
Published: October 22, 2012

   dx.doi.org/10.1021/jp307406j | *J. Phys. Chem. C* 2012, 116, 24107−24114

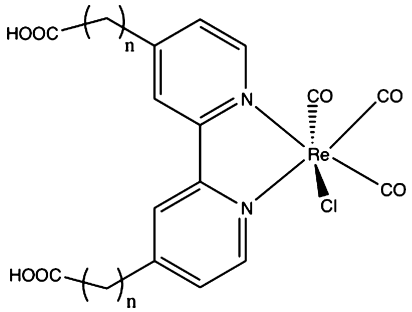

Figure 1. Schematic structure of ReC*n*A, where *n* refers to the number of methylene linkers between the carboxylate group and bipyridine ring.

varying lengths (*n*-CH_2 units).[21−23] These complexes have been shown to inject electrons into the semiconductor at different rates depending on the value of *n*.[22,23] However, it is currently unclear if this rate dependence is due to a change in the average orientation of these complexes on the semiconductor surface as *n* increases. A change in molecular conformation could also be expected to affect the overall catalytic efficiency of such molecules, since the catalytic Re center must be free to coordinate a CO_2 molecule in working systems. Therefore, a study of the average molecular orientation of the ReC*n*A family, with increasing *n*, may elucidate the effect orientation plays on electron transfer and catalytic capability.

In this work, we have investigated the average molecular orientation of the ReC*n*A series (n = 0−4) on a rutile TiO_2(001) single crystal using a combination of phase-sensitive vibrational sum frequency generation spectroscopy (PS-VSFG) and density functional theory (DFT) calculations. The (001) surface was chosen for its C_4 symmetry, which simplifies the analysis compared to less symmetric TiO_2 cuts.

II. THEORY

The theory of sum frequency generation has been examined in detail elsewhere and thus will be only briefly outlined here.[6−8,24] In a typical vibrational sum frequency generation spectroscopy experiment, two optical beams, one of fixed narrowband visible frequency ω_{vis} and one of tunable and/or broadband infrared frequency ω_{IR}, are overlapped spatially and temporally at an interface. This generates a third coherent optical beam from the surface with a frequency equal to the sum of the two incident frequencies ($\omega_{SF} = \omega_{vis} + \omega_{IR}$), the intensity of which is given by[6,24−27]

$$I(\omega_{SF}) \propto |\chi^{(2)}_{eff} E_{vis}(\omega_{vis}) E_{IR}(\omega_{IR})|^2 \quad (1)$$

where $E_{vis}(\omega_{vis})$ and $E_{IR}(\omega_{IR})$ are two incident electric fields. The effective nonlinear susceptibility $\chi^{(2)}_{eff}$ takes the form of

$$\chi^{(2)}_{eff} = [\hat{e}(\omega_{SF})\cdot L(\omega_{SF})]\cdot\chi^{(2)}:[L(\omega_{vis})\cdot\hat{e}(\omega_{vis})] \times [L(\omega_{IR})\cdot\hat{e}(\omega_{IR})] \quad (2)$$

where $\hat{e}(\omega)$ and $L(\omega)$ are the unit polarization vectors and Fresnel factors at frequency ω, respectively, and $\chi^{(2)}$ is the nonlinear susceptibility tensor. $\chi^{(2)}$ can typically be decomposed into a sum of resonant ($\chi^{(2)}_R$) and nonresonant ($\chi^{(2)}_{NR}$) terms:

$$\chi^{(2)} = \chi^{(2)}_R + \chi^{(2)}_{NR} \quad (3)$$

The nonresonant portion of the susceptibility may result from both the interfacial molecules and the media on either side of the interface, and is typically considered to be the result of electronic transitions. The resonant portion of the nonlinear susceptibility results solely from the interfacial molecules and is a measure of their response to the incident electric fields. More specifically, $\chi^{(2)}_R$ is defined as the macroscopic average of the microscopic molecular hyperpolarizability elements β. The elements of the resonant portion of $\chi^{(2)}$ are thus given by

$$\chi^{(2)}_{ijk} = N_s \sum_{\alpha\beta\gamma=abc} \langle R(\psi)R(\theta)R(\phi)\rangle \beta_{\alpha\beta\gamma} \quad (4)$$

where N_s is the molecule number density, $R(\Omega)$ is a rotation transformation matrix used to transform from the molecular coordinates (a, b, and c) to the laboratory coordinates (x, y, and z) through the Euler angles (θ, ϕ, and ψ), and the operator $\langle\ \rangle$ denotes an orientational ensemble average. The hyperpolarizability elements take the form[24,28]

$$\beta_{\alpha\beta\gamma}(-\omega_{sum};\ \omega_{vis},\ \omega_{IR}) = \frac{1}{2\hbar}\sum_n \frac{M_{\alpha\beta}T_\gamma}{(\omega_n - \omega_{IR} - i\Gamma_n)} \quad (5)$$

where ω_{IR} is the frequency of the incident tunable infrared beam, ω_n and Γ_n are the frequency and damping constant of the nth vibrational mode, respectively, and $M_{\alpha\beta}$ and T_γ are the Raman and infrared transition moments, respectively, of the nth vibrational mode. The sum is over all vibrational modes of the interfacial molecules.

In the case where $\chi^{(2)}_R$ is much larger than $\chi^{(2)}_{NR}$, the projection of a particular vibrational mode on the laboratory axis can be determined by monitoring the SFG response as a function of the incident and generated polarizations. However, when $\chi^{(2)}_R$ is equal to or smaller than $\chi^{(2)}_{NR}$, it can be difficult to accurately quantify each contribution, prohibiting orientation analysis. This is the case for ReC*n*A/TiO_2(001) when n = 1−4; we speculate that this is due to a lower SFG response from the ReC*n*A (n = 1−4) systems compared to the ReC0A system, causing the resonant signal to be comparable to the nonresonant response from the TiO_2 substrate. In this case, phase-sensitive VSFG (PS-VSFG) can be used to distinguish between the resonant and nonresonant contributions.

In the PS-VSFG detection scheme used in this study, the phase and amplitude of the sample SF field are measured by combining it with a stable broad "local oscillator" field, which is separated by a time τ with respect to the sample SF signal. The intensity of the PS-VSFG signal is thus

$$\begin{aligned} I_{PS\text{-}VSFG} &= |\chi^{(2)}_s E_{vis}E_{IR} + \chi^{(2)}_{lo} E_{vis}E_{IR} e^{i2\pi\omega\tau}|^2 \\ &= |\chi^{(2)}_s E_{vis}E_{IR}|^2 + |\chi^{(2)}_{lo} E_{vis}E_{IR}|^2 \\ &\quad + 2\mathrm{Re}[\chi^{(2)}_{lo}\chi^{(2)}_s {E_{vis}}^2 {E_{IR}}^2 e^{i2\pi\omega\tau}] \end{aligned} \quad (6)$$

The relevant spectral information is contained in the so-called "cross-term", given by the last term in eq 6. The cross-term can be separated from the other contributions through careful signal processing.[29,30] Specifically, the spectrum is first inverse Fourier transformed into the time domain, where the $\mathrm{Re}[\chi^{(2)}_s\chi^{(2)}_{lo}{E_{vis}}^2{E_{IR}}^2 e^{i2\pi\omega\tau}]$ cross-term is separated from the other terms by a time τ and can thus be isolated by application of a boxcar function. The result is then Fourier transformed back into the frequency domain to yield

$$I_{\text{PS-VSFG}} = \chi_{\text{lo}}^{(2)}\chi_{\text{s}}^{(2)}E_{\text{vis}}{}^{2}E_{\text{IR}}{}^{2}e^{i2\pi\omega\tau} \quad (7)$$

In order to extract the relevant molecular information contained in $\chi_{\text{s}}^{(2)}$, the resulting spectrum must be normalized against a standard sample of known $\chi^{(2)}$. In this experiment, a gold film was used. As gold has no resonances in the investigated spectral region, its response is real and flat over this wavelength range and $\chi_{\text{Au}}^{(2)}$ can be considered a constant. The sample spectrum can thus be normalized by the processed gold spectrum to yield the $\chi_{\text{s}}^{(2)}$ of interest:

$$\frac{\chi_{\text{lo}}^{(2)}\chi_{\text{s}}^{(2)}E_{\text{vis}}{}^{2}E_{\text{IR}}{}^{2}e^{i2\pi\omega\tau}}{\chi_{\text{lo}}^{(2)}\chi_{\text{Au}}^{(2)}E_{\text{vis}}{}^{2}E_{\text{IR}}{}^{2}e^{i2\pi\omega\tau}}e^{i\theta} = \frac{\chi_{\text{s}}^{(2)}}{\chi_{\text{Au}}^{(2)}}e^{i\theta} \quad (8)$$

The $e^{i\theta}$ term is included to describe any phase difference between the sample and gold spectra which can result from slightly different positioning between the ReC*n*A/TiO_2 and gold samples. This can be subsequently corrected by application of a phasing factor.

The phase-sensitive detection scheme has the advantage that $\chi_{\text{s}}^{(2)}$ is directly measured such that the real and imaginary parts can be separated and investigated individually. This is vital to our experiment because the imaginary component of $\chi_{\text{s}}^{(2)}$ contains the vibrational information, while the real component is the derivative of the imaginary part plus any nonresonant responses. The average conformation of the molecules on the TiO_2 surface can then be deduced by modeling the imaginary SFG spectra as a function of molecular orientation.

III. EXPERIMENTAL AND COMPUTATIONAL METHODS

A. Sample Preparation. Rutile (001) TiO_2 single crystals were purchased from Commercial Crystal Laboratories, Inc. Prior to initial use, the crystals were sonicated in piranha solution (3:1 H_2SO_4/H_2O_2) for 1 h, followed by a Milli-Q (18 MΩ) water rinse. They were then placed in 1 M NaOH solution for 5 min, followed by another Milli-Q rinse. The crystals were then placed in 1 M HCl solution and exposed to UV radiation for 10 min. After the UV treatment, the crystals were rinsed with ethanol and immersed in an ethanol solution of the molecular adsorbates of interest, typically overnight. Prior to use, they were rinsed in ethanol to remove any nonadsorbed molecules remaining on the TiO_2 surface and allowed to dry in air. After preparation, the sensitized samples were stored in a dark, dry environment in order to preserve sample integrity for as long as possible.

B. Vibrational Sum Frequency Spectroscopy Setup. A detailed description of our experimental setup has been described elsewhere.[20] Briefly, the setup is based on a 1 kHz Spitfire Ti:sapphire regenerative amplifier system (Spectra Physics) producing 150 fs pulses at 800 nm with a pulse energy of 4 mJ. Half of the fundamental was used to pump a TOPAS-C OPA (Light Conversion) producing tunable IR pulses with energies of 10−20 μJ and a bandwidth of ∼200 cm^{-1}. The remaining 2 mJ of 800 nm was filtered with a narrowband interference filter (CVI F01-800-UNBLK-1.00) to narrow the spectral bandwidth to ∼12 cm^{-1} (1 nm) centered at 799 nm. The visible pulses were filtered to 2−10 μJ and combined with the IR at the sample. The polarization of the IR and visible beams was controlled to be p-polarized with polarizer/half-waveplate combinations. The reflected IR, visible, and SFG beams were then collected by a spherical mirror and refocused onto a piece of y-cut quartz in order to generate the local oscillator signal. A 2 mm thick CaF_2 window was used to delay the sample SFG beam by approximately 3.8 ps with respect to the local oscillator. The local oscillator and signal beams were collimated and filtered to remove any remaining visible and IR light before being focused onto the entrance slit of the imaging spectrograph (Acton Instruments SpectraPro 300i, 1200 groove/mm grating) and detected with an air-cooled CCD camera (Princeton Instruments VersArray 512B, 512 × 512 pixels) operating at −40.0 °C. Nonresonant PS-VSFG spectra from gold were obtained prior to collecting data for ReC*n*A/TiO_2(001) and used to reference the ReC*n*A/TiO_2 spectra. Homodyne-detected measurements could be performed using this setup by simply removing the local oscillator and CaF_2 phase plate.

C. Computational Methods. *SFG Spectrum Simulation.* The detailed information for simulating the SFG spectra using the *ab initio* parameters of polarizability derivatives and dipole moment derivatives with respect to normal mode coordinates can be found in our previous work.[31] In particular, the χ_{eff} signal here is calculated for the polarization combination of PPP,[6] referring to P-polarized sum-frequency field, P-polarized E_{vis}, and P-polarized E_{IR} in eq 1. For the SFG simulation, energy minimization and normal-mode analysis were performed for ReC0A at the density functional theory level, using the B3LYP functional and the LAN2DZ basis set. Dipole derivatives of each vibrational mode were obtained using the keyword "iop(7/33=1)" during a frequency calculation, and polarizability derivatives were obtained by performing the Raman vibrational analysis with the "polar" keyword. All of the above calculations were performed using the Gaussian 09 program.[32]

ReCnA/TiO_2 Binding Conformation Search and Geometry Optimization. We first oriented the plane of the bipyridine chromophore (without the Re metal, Cl and CO ligands) near the predicted orientation deduced from the PS-VSFG spectra within a reasonable distance with respect to the rutile TiO_2(001) surface. The TiO_2(001) surface was represented by a three-dimensional periodic slab with a vacuum in the [001] direction. Next, an optimization of the anchoring groups (i.e., $-CH_2-$ and $-COO^-$) with MM+ force field implemented in the Hyperchem computational package[33] was performed. The final structure was used as an initial guess for a full optimization using the density functional tight-binding (DFTB) theory implemented in DFTB+ computational code,[34] with the *tiorg-0-1*[35] and *mio-0-1*[36] DFTB parameter sets. After optimized at the DFTB level, DFT calculations were performed with the Vienna *Ab Initio* Simulation Package.[37] The PW91/GGA density functional[38] was used to describe electron exchange and correlation. A plane-wave basis truncated with a 400 eV cutoff was used in all calculations as well as a single *k*-point sampling and ultrasoft Vanderbilt pseudopotentials.[39] The default convergence criteria were used for both the electronic energy and nuclear geometry optimizations.

IV. RESULTS AND DISCUSSION

The homodyne- and phase-sensitive-detected VSFG spectra of the ReC0A complex on TiO_2(001) in the carbonyl stretching region are shown in Figure 2. The FTIR spectrum of ReC0A on nanoporous TiO_2 is shown for comparison and exhibits three carbonyl bands: an in-phase symmetric a′(1) stretch ν_3 at 2040 cm^{-1} and an unresolved band consisting of an antisymmetric a″ stretch ν_2 (centered at ∼1939 cm^{-1}) and out-of-phase symmetric a′(2) stretch ν_1 (centered at ∼1910 cm^{-1}).[40,41] These carbonyl stretches are illustrated in Figure 3. The

dx.doi.org/10.1021/jp307406j | J. Phys. Chem. C 2012, 116, 24107−24114

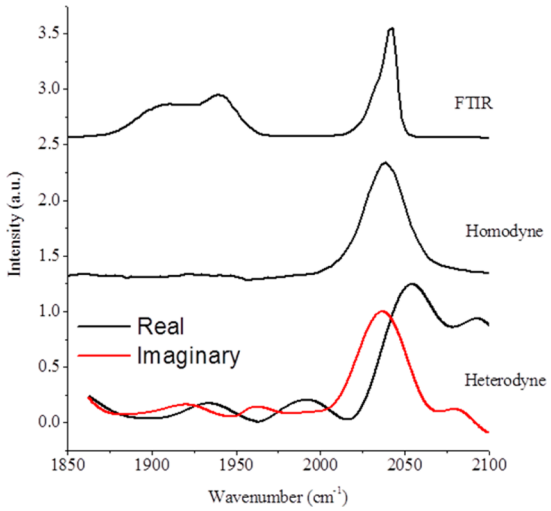

Figure 2. (top) FTIR spectrum of ReC0A on nanoporous TiO_2. (middle) Homodyne-detected and (bottom) phase-sensitive-detected VSFG spectra of ReC0A on single crystal TiO_2(001). Spectra are offset for clarity.

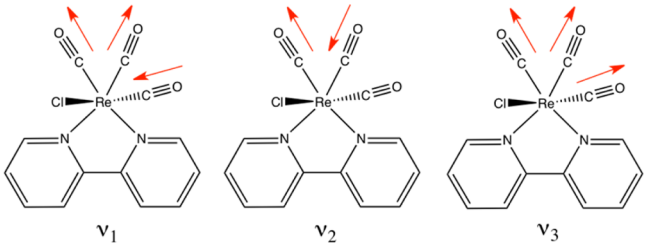

Figure 3. The three carbonyl stretches of ReC*n*A probed here: an out-of-phase symmetric a′(2) stretch (ν_1), an antisymmetric a″ stretch (ν_2), and an in-phase symmetric a′(1) stretch (ν_3).

homodyne SFG spectrum displays an intense peak at 2040 cm^{-1} with no other features observed at our signal-to-noise level. We assign this band to the a′(1) carbonyl stretch, and the band position is in good agreement with the FTIR spectrum. In the PS-VSFG spectra, the imaginary component reproduces the 2040 cm^{-1} feature again with no other bands observable at our signal/noise level. The real component of the PS-VSFG spectrum is the derivative of the imaginary spectrum, as would be expected for a homogeneous vibrational transition with no nonresonant contributions. The good agreement between the homodyne and phase-sensitive VSFG spectra indicates that the alternative detection scheme employed in PS-VSFG does not affect the experimental results.

The normalized PS-VSFG spectra of ReC*n*A (n = 0–4) are shown in Figure 4. Although ReC0A only exhibits the a′(1) carbonyl stretch at 2040 cm^{-1}, the imaginary spectra of all other complexes show peaks at 2030 and ~1900–1925 cm^{-1}. We assign the 2030 cm^{-1} band to the totally symmetric a′(1) carbonyl stretch. The redshift of this mode for ReC*n*A (n = 1–4) compared to ReC0A has been noted previously and can be attributed to increased electron density on the Re(I) metal center due to the insertion of the CH_2 spacers.[42] These spacers reduce the amount of electron delocalization into the carboxylate groups on the bipyridine ligand, thereby decreasing its electron withdrawing capabilities and increasing the electron density on the metal center.

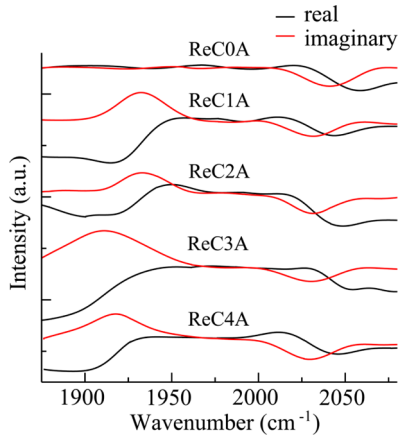

Figure 4. PS-VSFG spectra of ReC*n*A (n = 0–4) on single crystal TiO_2(001). Spectra are offset for clarity.

The hitherto unobserved low frequency band(s) can be assigned to the a″ and/or a′(2) modes. The significant SFG activity of either mode indicates that the extra methylene group(s) in the carboxyl linkers in ReC*n*A (n = 1–4) cause the orientation of the molecule on the TiO_2(001) surface to substantially deviate from normal. The a′(1) mode is out of phase relative to the a′(2) and a″ modes, and they thus show up as negative and positive peaks, respectively, in the PS-VSFG imaginary spectra. For each ReC*n*A (n = 1–4) spectrum, the real component of the phase-sensitive spectrum consists of the derivative of the imaginary spectrum on a broad, offset background, consistent with a large nonresonant response. The phase-sensitive detection scheme allows for the efficient separation of these two components, and thus a quantitative orientation analysis can be performed.

In order to determine the average molecular orientation for each complex on the TiO_2(001) surface, theoretical analysis was performed on the basis of an *ab initio* simulation of the imaginary traces of the PS-VSFG spectra corresponding to the intensity of the PPP effective second-order susceptibility.[6]

The intensity ratio (R_{amp}) between the low frequency peak (around 1915 cm^{-1}) and the high frequency peak (around 2030 cm^{-1}) for each complex in Figure 4 is listed in Table 1, together with the estimated error. For ReC0A, R_{amp} is zero, as no peak appears in the lower frequency peak region. For n = 1–4, the two peaks show opposite phases, with varying ratios of amplitudes.

Since the ReC*n*A complexes are attached to the TiO_2 rutile (001) surface, the change in the intensity ratios must originate from the orientation changes of the Re–bipyridine chromophores. As shown in Figure 5, the orientation of the Re–bipyridyl chromophores on the TiO_2 surface (represented by the surface Cartesian coordinates X, Y, and Z) are determined by three Euler transformation angles, θ, ϕ, and ψ, respectively. θ is the angle between the Z axis and the normal of the bipyridyl plane (the c axis), ψ is the angle between the long axis (the b axis) and the interaction line (the i axis) of the ab plane and the XY plane, and ϕ is the angle between the i axis and the Y axis. The specific molecular coordinate system within the ReC*n*A chromophore is chosen here for the convenience of illustrating the three orientation angles. The comparison to the molecular coordinate system used in our previous work[20] can be found in the Supporting Information. Due to the C_4 symmetry of the rutile (001) surface, the Re–bipyridyl

dx.doi.org/10.1021/jp307406j | J. Phys. Chem. C 2012, 116, 24107–24114

Table 1. Intensity Ratios (R_{amp}) of the Low-Frequency Peak around 1915 cm^{-1} Relative to the High-Frequency Peak around 2030 cm^{-1} for the ReC*n*A Complexes Shown in Figure 4

ReCnA, n =	0	1	2	3	4
R_{amp}	0 ± 0.01	−1.84 ± 0.17	−1.06 ± 0.05	−2.97 ± 0.11	−1.22 ± 0.07

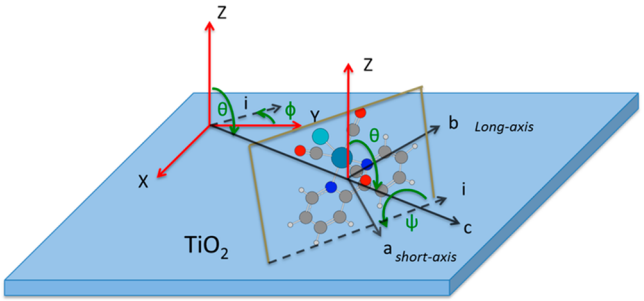

Figure 5. Schematic illustration of the orientation angles of a Re−bipyridine chromophore on the TiO_2 rutile (001) surface. Axes *X*, *Y*, and *Z* represent the Cartesian coordinates of the TiO_2 surface, and axes *a*, *b*, and *c* represent the Cartesian coordinates of the Re−bipyridine plane. Orientation angles θ, ϕ, and ψ are the Euler transformation angles between the two Cartesian coordinates. The *i* axis is the interaction line between the *ab* plane and the *XY* plane.

complexes can be distributed isotropically around the *Z* axis; thus, ϕ has an even distribution in the range 0−360°. The θ and ψ angles are to be determined for each complex.

We simulated the phase-sensitive spectra by independently scanning every 2° for the θ and ψ angles, and thus obtained the R_{amp} value for each simulated spectrum. A two-dimensional contour plot of R_{amp} versus θ and ψ is shown in Figure 6a, where the illustrated isolines 1−4 correspond to the experimental R_{amp} values of ReC*n*A with n = 1−4, respectively. For each ReC*n*A, all of the (θ, ψ) angles along the isoline are possible orientation angles. To identify which set of (θ, ψ) along the isoline can give a simulated PS-VSFG spectrum that agrees the best with the experimental spectrum, we divided the variational range of θ (0−180°) into smaller domains by scanning θ every 15°. For a particular θ, the variation of R_{amp} vs ψ is shown in Figure 6b (a similar plot with an interval of 2° for θ is provided in the Supporting Information), and for each ReC*n*A, a finite set of possible (θ, ψ) angles are identified by the interaction points between the predicted R_{amp} trend lines and the experimental R_{amp} line. For example, for R_{amp} = −1.22 in ReC4A, all the possible (θ, ψ) are (45°, 40°), (60°, 45°), (75°, 40°), (90°, 34°), (105°, 27°), and (120°, 8°).

For each ReC*n*A (n = 0−4), the experimental PS-VSFG spectrum was compared to the simulated spectra for the finite set of (θ, ψ) angles, and the particular set of (θ, ψ) whose simulated spectrum best matched the experimental spectrum yielded the proper orientation angles. The proper orientation angles for all the ReC*n*A (n = 0−4) complexes are given in Table 2. On the basis of the experimental errors of R_{amp} (see Table 1 and Figure 6b), the error in ψ was estimated, which is ±1° for all of the ReC*n*A complexes. We also estimated the error in θ at the proper angle points by examining the spectral changes as θ varies, and the error is ±2° (see Table 2). The estimated errors for θ and ψ are relatively small because R_{amp} is very sensitive to the variation of θ and ψ for our ReC*n*A (n = 0−4) systems. It should also be noted that, in the analysis above, we have assumed a delta function distribution of the orientation angles. As will be discussed below, there likely exist

Table 2. The Deduced Effective Orientation Angles (θ, ψ) for a Series of ReC*n*A (n = 0−4) Complexes Assuming a Delta Function Distribution of Angles[a]

ReC*n*A, n =	0	1	2	3	4
θ	75 ± 2°	105 ± 2°	75 ± 2°	45 ± 1°	45 ± 1°
η	15 ± 2°	−15 ± 2°	15 ± 2°	45 ± 1°	45 ± 1°
ψ	0 ± 1°	33 ± 1°	37 ± 1°	54 ± 1°	40 ± 1°

[a] η is the complementary angle of θ. The errors of the angles were estimated on the basis of the experimental errors of R_{amp}.

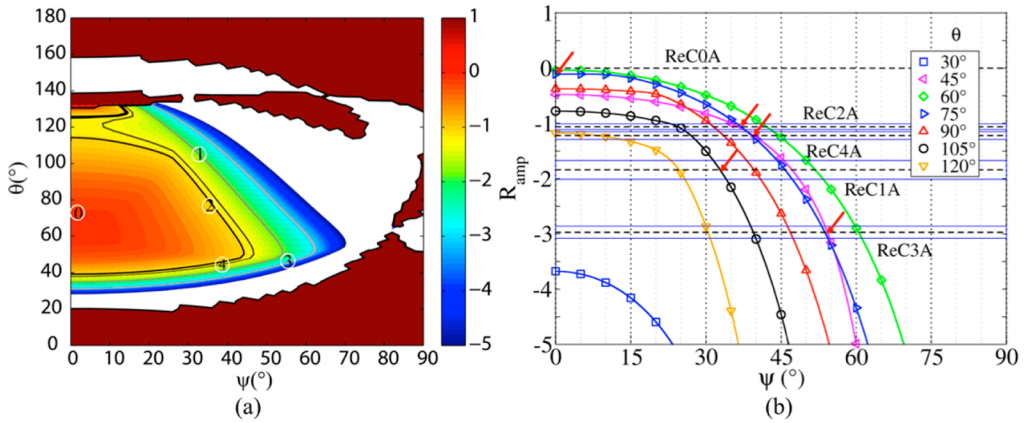

Figure 6. (a) Two-dimensional contour plot of R_{amp} (i.e., intensity ratios of the lower frequency peak around 1915 cm^{-1} to the higher frequency peak at 2030 cm^{-1}) versus orientation angles θ and ψ, obtained directly from simulated PS-VSFG spectra by scanning every 2° for θ and ψ, respectively. The solid isolines 1−4 correspond to the experimental R_{amp} values of ReC*n*A with n = 1−4, respectively. (b) Dependence of R_{amp} on ψ by scanning θ every 15°. The dashed lines illustrate the experimental R_{amp} values, and the two nearest blue lines parallel to a dashed line illustrate the error of the experimental R_{amp}. The arrows point to the particular sets of θ and ψ that yield the best-matching simulated spectra relative to the experimental spectra.

dx.doi.org/10.1021/jp307406j | J. Phys. Chem. C 2012, 116, 24107−24114

multiple conformations of adsorbates when n is large. Therefore, the deduced θ and ψ are the "effective" average angles for the orientations of an ensemble of ReCnA molecules on TiO_2 surfaces and their error bars do not reflect the range of all the possible orientation angles. To account for the distribution of orientation angles, we will perform comprehensive computational sampling of all the possible conformations (e.g., based on force-field molecular dynamics) in our future works.

The simulated SFG spectra with the proper orientation angles are shown in Figure 7, along with the corresponding

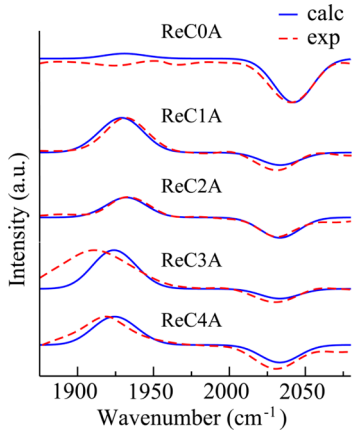

Figure 7. Simulated imaginary SFG spectra (blue solid traces) with the proper orientation angles (θ, ψ) for the ReCnA complexes (n = 0–4, from top to bottom), compared to the experimental imaginary PS-VSFG spectra (red dashed traces). Spectra are offset for clarity.

experimental PS-VSFG spectra. For each complex, we found that the simulated SFG spectrum matched fairly well with the experimental PS-VSFG spectrum. As shown by the deduced orientation angles in Table 2, both θ and ψ change as n increases from 0 to 4. For the convenience of discussion, the η angle (i.e., the angle between the ab plane and the Z axis, which is complementary to θ) is used as an equivalent to θ. η shows a tendency to increase with the growth of n. For n = 0–2, η remains relatively small, varying in the range of 15° in magnitude. For n = 3–4, η increases to 45°. The increase of η indicates that the Re–bipyridyl plane is tilted more toward the TiO_2 surface. Additionally, the ψ-angle is 0° when n = 0. As n increases from 1 to 4, the ψ-angle increases up to ~35° or higher. For n = 1 or 2, ψ is ~35°; for n = 3, ψ is 54°; and for n = 4, ψ is 40°.

We attribute the change in the orientation angles η and ψ to a conformational change of the two linker groups in ReCnA, where increasing the number of methylene groups in the linkers enhances the tilt of the bipyridyl ring relative to the TiO_2 surface. When n = 0, there is no $-CH_2-$ linker and the Re–bipyridyl ring is directly attached to the TiO_2 rutile (001) surface by the carboxylic anchoring groups. The conformation of the two carboxylic groups on the surface should be very similar, and thus, the length of the two anchoring groups (i.e., from the bipyridyl ring to the TiO_2 surface) is nearly equal. In this case, the ψ angle is zero, indicating the long axis of the bipyridyl plane is aligned parallel to the horizontal XY plane, while η = 15°, indicating the bipyridyl ring is tilted relative to the Z axis by 15°. Indeed, for n < 3, $|\eta|$ = 15°, indicating a small relative tilt of the bipyridyl ring. As n increases from 3 to 4, the average conformation of the two linkers can become very different as the σ-bonds between $-CH_2-$ groups can rotate freely. The length of the two linkers is thus unlikely to remain equal. Hence, both ψ and η deviate considerably from zero. The longer the linker groups become, the larger the length difference between the linkers could be. As a result, both ψ and η increase to the range of 33–54° when n = 3 or 4, indicating that both the short and long axes of the bipyridyl ring are tilted significantly relative to the TiO_2 surface. Given the larger number of possible conformations as the anchoring groups lengthen, we speculate that there are also a greater number of exhibited molecular orientations with increasing n. Since the experimental PS-VSFG spectra are the average of all molecular conformations, this may explain the spectral broadening at ~1915 cm^{-1} and poorer fit of the ReC3A and ReC4A complexes compared to ReCnA (n = 1–2).

We sampled a few possible binding conformations for the ReCnA complexes on the TiO_2 surface, and found the average orientation angles deduced from the phase-sensitive SFG spectra are indeed accessible. Figure 8 shows the optimized

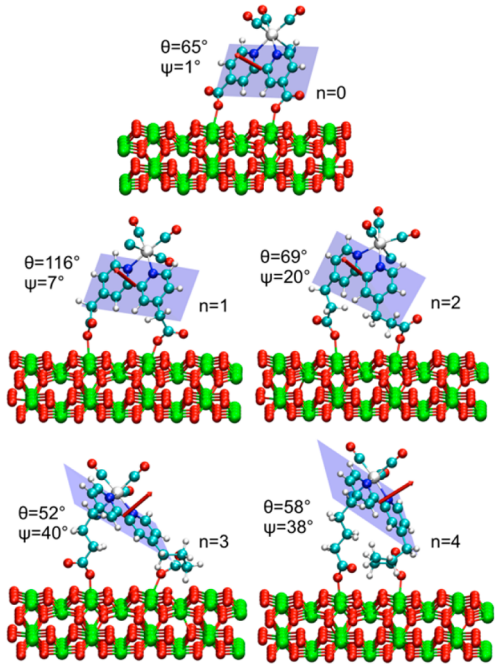

Figure 8. Optimized binding structures of ReCnA (n = 0–4), with orientation angles (θ and ψ) close to the average orientation angles deduced from the PS-VSFG spectra (see Table 2).

binding structures for each ReCnA (n = 0–4) complex on the TiO_2 rutile (001) surface, where the optimized orientation angles (see also Table S1 in the Supporting Information) are close to the deduced average angles in Table 2. The optimized conformations show an increase in the orientation angles of the complexes with increasing n, indicating that the ReCnA complexes tilt progressively more toward the TiO_2 surface as the methylene linkers lengthen. Additionally, Figure 8 illustrates that, as n increases from 0 to 4, the conformation difference between the two anchoring groups shows a tendency to enlarge. As a result, both the short and long axes of the bipyridyl plane are tilted considerably relative to the TiO_2 surface. These results verify our anticipated correlation between the bipyridyl ring tilt with the conformational change of the anchoring groups.

dx.doi.org/10.1021/jp307406j | J. Phys. Chem. C 2012, 116, 24107–24114

It should be pointed out that the simulated spectrum for ReC0A consistently overestimates the contribution of the two lower frequency modes. This experimental result is consistent with our previous investigation of ReC0A on TiO_2(001), in which the two lower frequency modes were not observed in the VSFG spectra.[20] We speculated that this may be due to a near-resonance effect originating from the nearby metal-to-ligand charge transfer (MLCT) band at ∼400 nm, which would enhance the Raman cross section of the a′(1) mode but not the a′(2) or a″ modes.[43] On the basis of this, a simplified model of the hyperpolarizability elements was used in the analysis. In the current work, the hyperpolarizability elements of free (unadsorbed) ReC0A were calculated directly according to eq 5, where the dipole and Raman polarizability derivatives were determined as described above. An analysis of the Raman polarizability derivatives as a function of the sum frequency wavelength indicates a negligible resonance effect of the MLCT transition, as seen in Figure S3 in the Supporting Information. However, these calculations do not account for the effects of the adsorption of ReC0A on TiO_2, which causes a red-shift in the MLCT transition (shown in Figure S4 in the Supporting Information). This red-shift can be attributed to the stabilization of the π^* orbital of bipyridine due to its strong interaction with the empty d orbitals of the bonded Ti atoms. This may push the system closer to near-resonance. These effects are expected to be much less significant for the ReC*n*A (n = 1−4) complexes, since the CH_2 spacer(s) reduce the amount of electron delocalization into the carboxylate groups, thus insulating the molecule from the effects of TiO_2 adsorption. If the ReC0A/TiO_2 system is approaching near-resonance as explained above, we can expect this to further enhance the difference between the high and low frequency modes, which is more consistent with the experimental results. This may also explain the much larger signal size for ReC0A on TiO_2(001) compared to ReC*n*A (n = 1−4).

CONCLUSION

Phase-sensitive vibrational sum frequency generation spectroscopy and density functional theory calculations have been used to determine the adsorption geometry of a family of model electrocatalysts, ReC*n*A (n = 0−4), on a single crystal TiO_2(001) surface. The imaginary SFG spectra for the ReC*n*A family (n = 1−4) show phase-sensitive SFG peaks in the regions of 2030 and 1915 cm^{-1}, originating from a combination of CO stretches. The intensity ratio (R_{amp}) of the two peaks in each PS-VSFG spectrum is associated with the average molecular orientation of the Re−bipyridyl complex relative to the TiO_2 surface. On the basis of the experimental R_{amp} values and simulated SFG spectra with varying orientation angles, the orientation angles for ReC*n*A (n = 0−4) have been determined. These orientation angles were found to be closely correlated with the increasing conformational difference between the two anchoring groups as they lengthen. Specifically, as the number of methylene groups in the anchoring groups increases, the short and long axes of the π-conjugated ring of the ReC*n*A complex tilt further toward the TiO_2 surface. We attribute this to the fact that the average conformation of the two linkers can become very different as n increases, as the σ-bonds between $-CH_2-$ groups can rotate freely. We additionally surmise that, given the larger number of average conformations as the anchoring groups lengthen, it is likely that there are a greater number of exhibited molecular orientations with increasing n, all of which are sampled in the PS-VSFG experiment. Increasing the length of the anchoring groups thus produces a more tilted and likely less ordered array of molecules on the semiconductor surface. This study demonstrates the ability to prepare an electrocatalyst−semiconductor system with a preferred average molecular arrangement based on the anchoring groups, though the ability to select a specific tilt angle may come at the cost of reducing overall systematic ordering.

ASSOCIATED CONTENT

Supporting Information

Figures showing the molecular coordinates used in this work and in ref 20, the dependence of R_{amp} on ψ, simulated PPP SFG intensities, experimental UV−visible absorption spectra and table showing orientation angles obtained by geometry optimization. This material is available free of charge via the Internet at http://pubs.acs.org.

AUTHOR INFORMATION

Author Contributions

[§]Equal contribution.

Notes

The authors declare no competing financial interest.

ACKNOWLEDGMENTS

V.S.B. acknowledges supercomputer time from NERSC and support from the Division of Chemical Sciences, Geosciences, and Biosciences, Office of Basic Energy Sciences of the U.S. Department of Energy (DE-FG02-07ER15909) and funding for development of computational methods from NSF CHE-0911520 and ECCS-040419. T.L. is supported by the Chemical Sciences, Geosciences and Biosciences Division, Office of Basic Energy Sciences, Office of Science, U.S. Department of Energy (DE-FG02-07ER-15906).

REFERENCES

(1) Prezhdo, O. V.; Duncan, W. R.; Prezhdo, V. V. *Acc. Chem. Res.* **2008**, *41*, 339−348.
(2) Adams, D. M.; Brus, L.; Chidsey, C. E. D.; Creager, S.; Creutz, C.; Kagan, C. R.; Kamat, P. V.; Lieberman, M.; Lindsay, S.; Marcus, R. A.; et al. *J. Phys. Chem. B* **2003**, *107*, 6668−6697.
(3) Kamat, P. V.; Meisel, D. *Curr. Opin. Colloid Interface Sci.* **2002**, *7*, 282−287.
(4) O'Regan, B.; Gratzel, M. *Nature* **1991**, *353*, 737−740.
(5) Gratzel, M. *MRS Bull.* **2005**, *30*, 23−27.
(6) Zhuang, X.; Miranda, P. B.; Kim, D.; Shen, Y. R. *Phys. Rev. B* **1999**, *59*, 12632−12640.
(7) Lambert, A. G.; Davies, P. B.; Neivandt, D. J. *Appl. Spectrosc. Rev.* **2005**, *40*, 103−145.
(8) Wang, H. F.; Gan, W.; Lu, R.; Rao, Y.; Wu, B. H. *Int. Rev. Phys. Chem.* **2005**, *24*, 191−256.
(9) Rao, Y.; Comstock, M.; Eisenthal, K. B. *J. Phys. Chem. B* **2006**, *110*, 1727−1732.
(10) Hawecker, J.; Lehn, J. M.; Ziessel, R. *J. Chem. Soc., Chem. Commun.* **1984**, 328−330.
(11) Hawecker, J.; Lehn, J. M.; Ziessel, R. *Helv. Chim. Acta* **1986**, *69*, 1990−2012.
(12) Yam, V. W. W.; Lau, V. C. Y.; Cheung, K. K. *Organometallics* **1995**, *14*, 2749−2753.
(13) Hayashi, Y.; Kita, S.; Brunschwig, B. S.; Fujita, E. *J. Am. Chem. Soc.* **2003**, *125*, 11976−11987.
(14) Fujita, E. H., Y.; Kita, S.; Brunschwig, B. S. Carbon Dioxide Utilization for Global Sustainability; 7th International Conference on Carbon Dioxide Utilization, 2004, Seoul, Korea.
(15) Fujita, E.; Muckerman, J. T. *Inorg. Chem.* **2004**, *43*, 7636−7647.

(16) Takeda, H.; Koike, K.; Inoue, H.; Ishitani, O. *J. Am. Chem. Soc.* **2008**, *130*, 2023−2031.
(17) Benson, E. E.; Kubiak, C. P.; Sathrum, A. J.; Smieja, J. M. *Chem. Soc. Rev.* **2009**, *38*, 89−99.
(18) Smieja, J. M.; Kubiak, C. P. *Inorg. Chem.* **2010**, *49*, 9283−9289.
(19) Cecchet, F.; Alebbi, M.; Bignozzi, C. A.; Paolucci, F. *Inorg. Chim. Acta* **2006**, *359*, 3871−3874.
(20) Anfuso, C. L.; Snoeberger, R. C.; Ricks, A. M.; Liu, W. M.; Xiao, D. Q.; Batista, V. S.; Lian, T. Q. *J. Am. Chem. Soc.* **2011**, *133*, 6922−6925.
(21) She, C.; Anderson, N. A.; Guo, J.; Liu, F.; Goh, W.; Chen, D.-T.; Mohler, D. L.; Tian, Z.-Q.; Hupp, J.; Lian, T. *J. Phys. Chem. B* **2005**, *109*, 19345−19355.
(22) Anderson, N. A.; Ai, X.; Chen, D.; Mohler, D. L.; Lian, T. *J. Phys. Chem. B* **2003**, *107*, 14231−14239.
(23) She, C.; Guo, J.; Irle, S.; Morokuma, K.; Mohler, D. L.; Zabri, H.; Odobel, F.; Youm, K.-T.; Liu, F.; Hupp, J. T.; et al. *J. Phys. Chem. A* **2007**, *111*, 6832−6842.
(24) Shen, Y. R. *The principles of nonlinear optics*; Wiley: New York, 1984.
(25) Feller, M. B.; Chen, W.; Shen, Y. R. *Phys. Rev. A: At., Mol., Opt. Phys.* **1991**, *43*, 6778−6792.
(26) Hirose, C.; Akamatsu, N.; Domen, K. *J. Chem. Phys.* **1992**, *96*, 997−1004.
(27) Rao, Y.; Tao, Y. S.; Wang, H. F. *J. Chem. Phys.* **2003**, *119*, 5226−5236.
(28) Moad, A. J.; Simpson, G. J. *J. Phys. Chem. B* **2004**, *108*, 3548−3562.
(29) Pool, R. E.; Versluis, J.; Backus, E. H. G.; Bonn, M. *J. Phys. Chem. B* **2011**, *115*, 15362−15369.
(30) Mondal, J. A.; Nihonyanagi, S.; Yamaguchi, S.; Tahara, T. *J. Am. Chem. Soc.* **2010**, *132*, 10656−10657.
(31) Xiao, D.; Fu, L.; Batista, V. S.; Yan, E. C. Y. *J. Mol. Biol.* **2012**, *421*, 537−547.
(32) Frisch, M. J.; Trucks, G. W.; Schlegel, H. B.; Scuseria, G. E.; Robb, M. A.; Cheeseman, J. R.; Scalmani, G.; Barone, V.; Mennucci, B.; Petersson, G. A.; et al. *Gaussian 09*, revision A.1 ed.; Gaussian, Inc.: Wallingford, CT, 2009.
(33) *Hyperchem(TM) Professional 7.51*; Hypercube, Inc.: Gainesville, FL.
(34) Aradi, B.; Hourahine, B.; Frauenheim, T. *J. Phys. Chem. A* **2007**, *111*, 5678−5684.
(35) Dolgonos, G.; Aradi, B.; Moreira, N. H.; Frauenheim, T. *J. Chem. Theory Comput.* **2010**, *6*, 266−278.
(36) Elstner, M.; Porezag, D.; Jungnickel, G.; Elsner, J.; Haugk, M.; Frauenheim, T.; Suhai, S.; Seifert, G. *Phys. Rev. B* **1998**, *58*, 7260−7268.
(37) Kresse, G.; Furthmuller, J. *Phys. Rev. B* **1996**, *54*, 11169−11186.
(38) Perdew, J. P. In *Electronic Structure of Solids '91*; P. Ziesche, H. E., Ed.; Akademie Verlag: Berlin, 1991; pp 11−20.
(39) Vanderbilt, D. *Phys. Rev. B* **1990**, *41*, 7892−7895.
(40) Wang, Y.; Asbury, J. B.; Lian, T. *J. Phys. Chem. A* **2000**, *104*, 4291−4299.
(41) Gamelin, D. R.; George, M. W.; Glyn, P.; Grevels, F. W.; Johnson, F. P. A.; Klotzbucher, W.; Morrison, S. L.; Russell, G.; Schaffner, K.; Turner, J. J. *Inorg. Chem.* **1994**, *33*, 3246−3250.
(42) Asbury, J. B.; Hao, E.; Wang, Y.; Lian, T. *J. Phys. Chem. B* **2000**, *104*, 11957−11964.
(43) Waterland, M. R.; Howell, S. L.; Gordon, K. C. *J. Phys. Chem. A* **2007**, *111*, 4604−4611.